Available online at www.sciencedirect.com
SCIENCE DIRECT
Biochimica et Biophysica Acta 1757 (2006) 90–105
BIOCHIMICA ET BIOPHYSICA ACTA
BBA
http://www.elsevier.com/locate/bba

Review

Design and engineering of photosynthetic light-harvesting and electron transfer using length, time, and energy scales

Dror Noy [1], Christopher C. Moser, P. Leslie Dutton *

Johnson Research Foundation, Department of Biochemistry and Biophysics, University of Pennsylvania, Philadelphia, PA 19104, USA

Received 17 September 2005; received in revised form 16 November 2005; accepted 21 November 2005
Available online 11 January 2006

Abstract

Decades of research on the physical processes and chemical reaction-pathways in photosynthetic enzymes have resulted in an extensive database of kinetic information. Recently, this database has been augmented by a variety of high and medium resolution crystal structures of key photosynthetic enzymes that now include the two photosystems (PSI and PSII) of oxygenic photosynthetic organisms. Here, we examine the currently available structural and functional information from an engineer's point of view with the long-term goal of reproducing the key features of natural photosystems in de novo designed and custom-built molecular solar energy conversion devices. We find that the basic physics of the transfer processes, namely, the time constraints imposed by the rates of incoming photon flux and the various decay processes allow for a large degree of tolerance in the engineering parameters. Moreover, we find that the requirements to guarantee energy and electron transfer rates that yield high efficiency in natural photosystems are largely met by control of distance between chromophores and redox cofactors. Thus, for projected de novo designed constructions, the control of spatial organization of cofactor molecules within a dense array is initially given priority. Nevertheless, constructions accommodating dense arrays of different cofactors, some well within 1 nm from each other, still presents a significant challenge for protein design.

Keywords: Chlorophyll; Electron tunneling; Förster resonance energy transfer; Reaction center; Redox chain

1. Introduction

The initial steps of photosynthesis, light energy transfer and charge separation, are probably the best-characterized biological energy conversion processes. This is the result of extensive research, particularly in the past 50 years, which has capitalized on timely major theoretical, experimental and technological breakthroughs [1,2]. Experimentally, photosynthetic enzymes enjoy the unique property of permitting the initiation of truly single-turnover catalytic cycles with short light flashes at temperatures from 1 K to above 300 K, as well as providing distinct fluorescence and absorbance spectroscopic markers for probing catalytic intermediates. Therefore, studies of physical processes and chemical reaction-pathways in these enzymes have benefited from advances in optical spectroscopy and pulsed flash and laser technology.

Already in the 1930s, primitive photography flash lamp technology led to the formulation of the photosynthetic unit (PSU) concept through the pioneering experiments of Emerson and Arnold [3,4] and their explanation by Gaffron and Wohl [5]. Later, seminal work by Duysens in the 1950s developed difference spectrophotometry to show that bacterial PSUs consist of about 200 "antenna" or light-harvesting (LH) bacteriochlorophylls (BChls) and one "reaction center" (RC) or trapping pigment [6]. He suggested that excitation energy rapidly migrates via the Förster resonance energy transfer mechanism from the LH pigment into the RC where the photochemical steps are initiated. Following early work on light-activated events in photosynthetic organisms at cryogenic temperatures [7,8], early laser technology led DeVault and Chance to discover biological electron tunneling in 1966 [9], which prompted substantial theoretical efforts and ever-faster spectroscopic techniques. The determination of a bacterial RC structure at near atomic-resolution by Deisenhoffer, Michel and

* Corresponding author. Tel.: +1 215 898 5668; fax: +1 215 573 2235.
E-mail address: dutton@mail.med.upenn.edu (P.L. Dutton).
[1] Current address: Department of Structural Biology, Weizmann Institute of Science, Israel.

0005-2728/$ - see front matter © 2005 Elsevier B.V. All rights reserved.
doi:10.1016/j.bbabio.2005.11.010

Huber in early 1980s marks the next historical breakthrough as the first membrane protein structure ever determined [10]. This was followed by an exponential burst of high-resolution crystal structures of transmembranal proteins including LH [11–15], RC [16–22] and redox affiliated proteins from a variety of photosynthetic organisms [23–26]. At the same time, genetic and other biochemical methods were developed to provide means for local and specific protein structure alterations [27–31] and cofactors exchange [32–37], whereas lower resolution structural techniques such as electron cryo-microscopy [38–44] and atomic force microscopy (AFM) [45–49] provide additional valuable information about the higher order organization of protein complexes within the photosynthetic membrane.

The current combination of laser technology that probes several femtosecond photoexcitation processes both in bulk solution and in single molecules with high resolution structural information of native and modified photosystems, and state of the art theoretical methods and thermodynamic analysis provide a well-established framework for describing biological electron transfer processes [50]. This wealth of physical, chemical and functional information derived from over 70 years of research and newly emerging structures, as well as growing public interest in renewable energy sources and alternatives to fossil fuels, encourage many to turn to photosynthetic proteins as inspiration for effective and reliable solar energy conversion systems.

Here, we review the current knowledge of photosynthetic electron and energy transfer processes from an engineer's perspective. We have endeavored to delineate the underlying chemical and physical principles of energy and electron transfer processes in PSUs and their translation into useful engineering and construction guidelines for designing custom solar energy conversion systems. In this regard, we follow our recent survey of electron transfer principles in natural proteins of photosynthesis and respiration [51]. The same simple arguments relating relaxation times, energy, and the dominance of distance are used here as engineering guidelines for designing competent LH and RC systems, and coupling them into an efficient PSU. More specifically, we ask what are the engineering principles that are essential for PSU operation at near unit quantum yield, what governs the selected engineering efficiency, what is the energetic tolerance against the onset of failure, and how do the engineering principles challenge the construction and assembly of PSUs?

2. Overview of length scales in photosynthetic light-harvesting and electron transfer

Fig. 1 describes typical relays of membrane proteins in photosynthetic bacteria, plants and algae in which light energy is captured by a network of LH proteins and transferred to an RC protein that catalyzes electron tunneling-mediated charge separation and generates transmembranal electric potential. Redox connection of the RC with neighboring membrane oxidoreductases such as cytochrome bc_1 or b_6f is then mediated through molecular diffusion of substrates and products, principally quinones within the membrane, and cytochrome *c* or plastocyanin peripheral to the membrane. Cytochrome bc_1/b_6f, like the RC, promotes transmembranal charge separation and contributes to the build up of an electrochemical potential gradient of protons. This electrochemical potential gradient ultimately provides the driving force for the majority of biochemical reactions in the cell, including the dark reactions of photosynthesis.

Although photosynthetic proteins are large and complex, it appears that the engineering that has been favored by blind natural selection is comparatively simple and resilient, and does not require an atom-by-atom examination to appreciate its functional design. Instead, we can begin by considering how nature has exploited the fundamental physical processes that are involved in the energy conversion relay. Each of these processes exhibits distinctive rates, which impose time constraints on the integrated design. Engineering guidelines for effective LH and RC proteins can therefore be derived from the length and energy scales that are associated with these processes (Fig. 2).

The first length scale (Fig. 2A) is associated with the rate of photon absorption. Einstein's theory of light absorption sets an upper boundary for the absorption cross section, σ', of ~10 Å^2 for a single UV-Visible absorption band of small organic molecules [52]. The cross section will depend on the photon energy, E. Typically $\sigma'(E)\approx 0.1$–2 Å^2 for the strongest absorption bands of photosynthetic pigments. The rate of photon absorption will also depend on the flux of photons in the spectrum of the solar irradiance, $\phi(E)$. However, out of all the photons absorbed, the "useful" photons are limited to those above an energetic threshold, $E_{\min}$, set according to the driving force of the charge separation reaction. The effect of this energy scale is to constrain the power output for any solar energy conversion device: the higher the $E_{\min}$ the slower the rate of the total absorption. The absorption rate of these "useful" photons is given by

$$K_{\text{abs}} = \int_{E_{\min}}^{\infty} \phi(E)\sigma'(E)\mathrm{d}E. \tag{1a}$$

Another useful way to look at the absorption rate of useful photons is to consider the effective total cross section for useful photons, $\sigma^E(E_{\min})$, given by

$$\sigma^E(E_{\min}) = \frac{\int_{E_{\min}}^{\infty} \phi(E)\sigma'(E)\mathrm{d}E}{\int_0^{\infty} \phi(E)\mathrm{d}E}, \tag{1b}$$

then,

$$K_{\text{abs}} = \sigma^E(E_{\min}) \int_0^{\infty} \phi(E)\mathrm{d}E = \sigma^E(E_{\min})\phi_{\text{total}}, \tag{1c}$$

where ϕ_{total} is the total flux of incident solar photons. Obviously, ϕ_{total} changes according to environmental conditions (time of day, season, geographic location). A useful estimate is $\phi_{\text{total}}=4\times10^{21}$ photons s^{-1} m^{-2} obtained by interating the standard reference solar spectral irradiance at Air Mass 1.5 (ASTM G-173-03) [53]. For consistency with the other length scales, we define a length parameter, r, such that $\sigma^E=r^2$ hence,

$$K_{\text{abs}} \approx 40\sigma^E(E_{\min}) = 40r^2, \tag{1d}$$

where r is in units of Å. Typically, r for a single Chl molecule is ~0.3 Å and the maximal photon absorption rate for a single

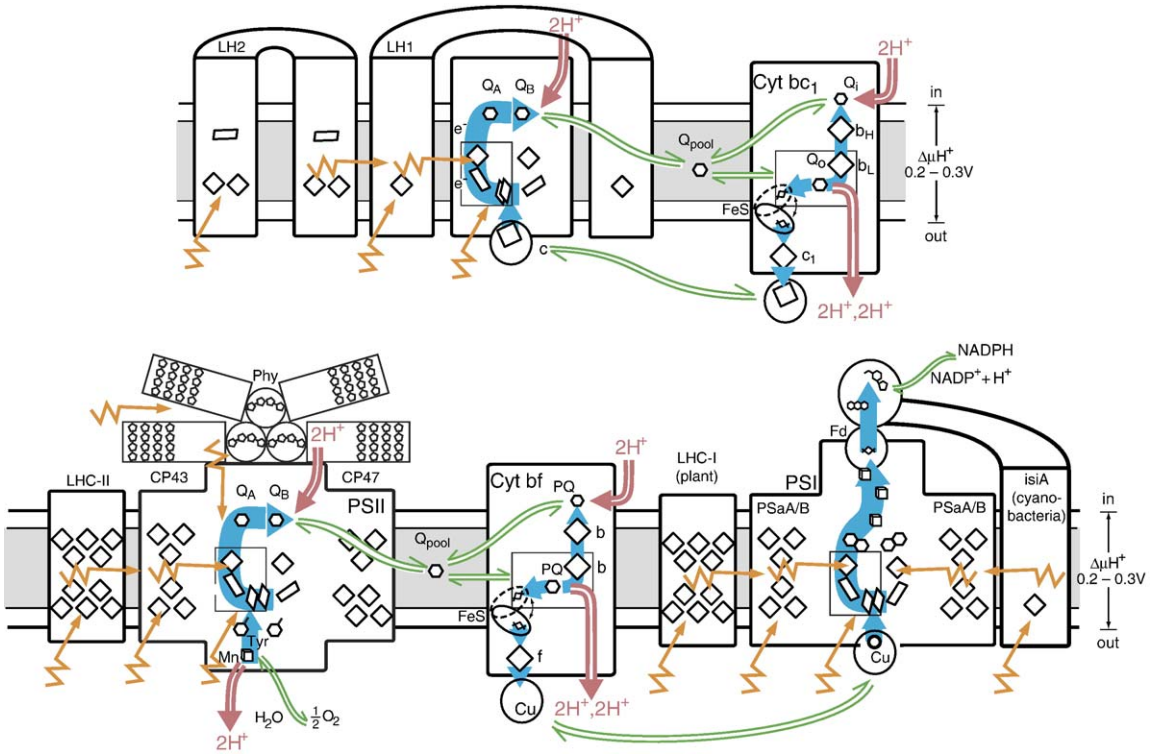

Fig. 1. Schematic representation of cofactors in light harvesting, reaction center, and bc_1 proteins of photosynthetic organisms. First row: purple bacterial membrane; second row: plant membranes with photosystem I (PSI), photosystem II (PSII) and b_6f analogous to bc_1 complex; light-energy excitation or energy transfer (orange arrows) between (bacterio)chlorophylls (diamonds) leads eventually to charge separation in reaction centers (gray boxes) and electron tunneling (blue arrows) from center to center in a chain across the membrane (gray, low dielectric region) to create a transmembranal electric field. Proton binding and release (red arrows) occurs at chains terminating in quinones (hexagons), generating a transmembranal proton gradient. In addition, reduced quinone and oxidized cytochrome *c* or plastocyanin diffuse (green arrows) to connect membrane complexes.

pigment is therefore ~4 s^{-1} under standard solar irradiance conditions. Hence, a PSU comprising 30–300 molecules is mandatory if typical biological catalysis rates of 10^2–10^4 s^{-1} (grey band in Fig. 2) are to be achieved. Notably, from our engineer's perspective, the choice of E_{min} is arbitrary as long as E_{min} provides enough free energy to drive the photochemical reaction. It is possible to trade low potentials by high current without compromising the available power [54].

Electron transfer (ET) defines the second length scale (Fig. 2B) which is associated with electron tunneling. Tunneling parameters are reasonably well estimated by the simple empirical expression

$$\log K_{et} = \begin{cases} 15 - 0.6r - \dfrac{3.1(\Delta G + \lambda)^2}{\lambda}, \Delta G<0 \\ 15 - 0.6r - \dfrac{3.1(\Delta G + \lambda)^2}{\lambda} - (\Delta G/RT)\log e, \Delta G>0 \end{cases} \quad (2)$$

where K_{et} is in units of s^{-1}, r is the edge-to-edge distance between redox cofactors in Å, and ΔG and λ are the reaction free energy and reorganization energy, respectively in units of eV. The free energy dependence of the electron-tunneling rate gives rise to an associated energy scale, whereby for any characteristic time and free energy, there is a maximum distance over which tunneling can extend [50,55,56]. This is true for both the traditional exergonic ($\Delta G<0$) electron transfers, as well as the endergonic ($\Delta G>0$) or uphill electron transfers [55]. ET through a series of redox cofactors, which may include energetically unfavorable ET steps, can take place within a given time as long as the uphill electron transfer is followed eventually by a favorable downhill electron transfer. Indeed, endergonic electron transfers through intermediates hundreds of meV uphill can take place faster than typical enzymatic turnover times provided the redox centers are closer than 14 Å (edge to edge). The shorter the distance, the more energetically unfavorable the electron transfer intermediate can be.

The third length scale (Fig. 2B, left) is associated with excitation energy transfer (EET), which occurs primarily via Coulomb (dipole–dipole) interactions between donor and acceptor chromophores that decays with a $1/r^6$ dependence on distance [58,59]. The process can be described, to a first order approximation, by Förster's equation,

$$K_{eet} = k_f \left(\frac{r_o}{r}\right)^6 \quad (3)$$

where k_f is the radiative rate constants of the donor, and r_o is a critical radius at which energy transfer is 50% efficient. Here, donor and acceptor are viewed as point dipoles and r is the distance between them. The critical Förster radius, r_o, depends on energetic parameters such as the overlap between donor and acceptor, and the relative orientation of their transition dipoles.

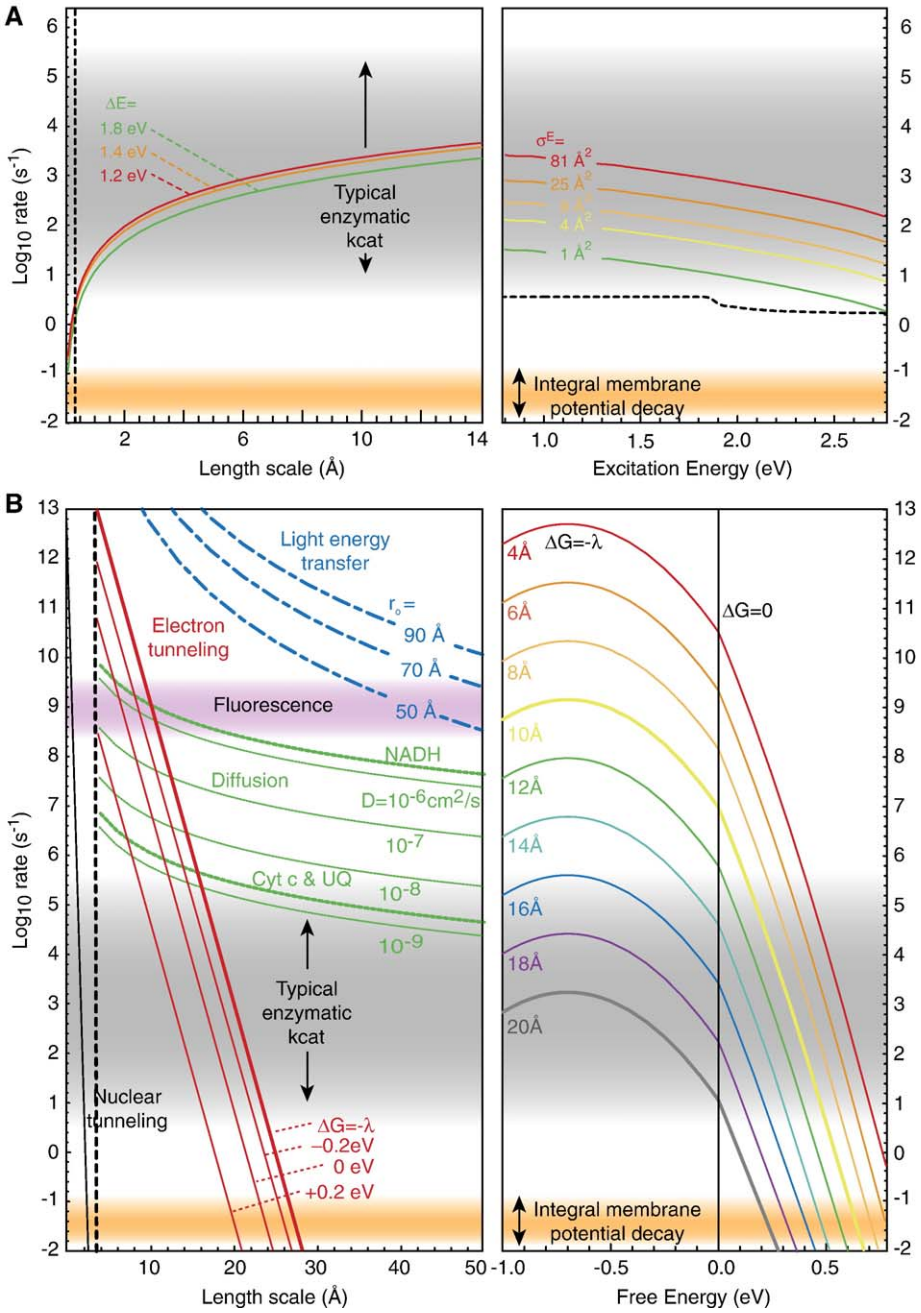

Fig. 2. Fundamental processes in photosynthesis display characteristic rate/distance/energy dependencies that dictate the basic design of the LH and ET complexes. (A) The rate of light absorption depends on the flux and spectral distribution of photons (estimated by the reference solar spectral irradiance at Air Mass 1.5 [53]), the integrated absorption cross-section (σ^E) and the excitation energy (ΔE) according to Eq. (1). Left and right graphs represent length and energy scales for photon absorption rate, respectively. The length parameter, r is defined by $\sigma^E = r^2$. The energy parameter is the excitation energy of the primary electron donor, which corresponds to the integration limit, E_{min}, in Eq. (1) and sets a cutoff value for useful photons. The dashed black line on the right panel indicates the photon absorption rate of Chl *a* in diethyl ether and the vertical dashed black line on the left marks the respective r for $E_{min} < 1.8$ eV. (B) Left graph represents length scales for light energy transfer (blue), electron tunneling (red) and proton tunneling (black), and diffusion (green). Fluorescence decay times (purple), enzymatic turnover times (gray) and membrane potential decay (orange) represent basic engineering time constraints. Fluorescence heralds the end of the energy transfer time domain. Right graph represents the energy scale of electron tunneling whereby the energy parameter is the free energy of redox reaction that reaches a maximum when the exergonic energy release matches the reorganization energy (λ) for the electron transfer, here illustrated for a typical value of 0.7 eV. The gray band spans the range of catalytic rates (K_{cat}) of the large majority of enzymes. The lower orange band is typical trans-membranal ion leakage rates that collapse the gradients of potential ($\Delta\psi$) and pH (ΔpH), and other electrochemical gradients [57]; such a slow decay rate does not present a threat to normal physiological function.

Typical r_o values for photosynthetic pigments are 50–100 Å [58].

The point dipole approximation becomes less reliable as distances between chromophores become shorter than 10 Å as is often the case for the densely packed pigment arrays of LH proteins. Therefore, other expressions must be sought to describe energy transfer between strongly coupled individual chromophores and for delocalized excitation. Recently

available detailed structures of LH proteins prompted the development of more elaborate computational methods, which have provided much deeper insights into the mechanisms of energy migration and trapping in LH proteins [60–62]. In contrast to earlier views, it is now recognized that excitation energy "funneling" from higher to lower energy sites of excitonically coupled pairs is not required for efficient energy transfer under conditions of strong coupling and long-range delocalization [63–65]. In fact, under these conditions thermal disorder promotes energy transfer because it allows better spectral overlap between chromophores with different energies.

3. Engineering insights from natural photosystem design

3.1. Light absorption

Regardless of specific architecture, any solar energy conversion system must maintain sufficient photon throughput to keep up with the rates of subsequent transfer processes. The global limitations of incoming photon flux through one molecule (Fig. 2A) may be compensated for by approximately 100 pigment molecules to provide an absorption cross section that is large enough to maintain a single elementary transfer process (e.g. one electron or proton transfer) at a typical enzymatic rate of 10^3 s^{-1}. As shown in Table 1, photosynthetic enzymes may comprise pigments almost up to 40% of their total mass. The types of pigment and their proportions in the mixture are predominantly determined by the prevailing light wavelengths at the organism's habitat.

Lifetime and distance considerations impose important constraints on the pigment packing architecture. Solutions of chlorophylls (Chls) in fluid solvents, monolayers, lipid bilayers and even rigid polymer matrices exhibit significant reduction in excited state lifetimes and fluorescence yield that is proportional to the pigment concentration. This concentration-quenching phenomenon is pronounced even at much lower concentrations than those typical of pigments in photosynthetic membranes. Beddard and Porter [66] suggested that quenching is caused by Förster-type energy transfer to pairs of Chls closer than a critical distance of 10 Å. Such Chl dimers provide many non-radiative channels for dissipating excitation energy thus becoming non-fluorescent traps [67]. Beddard [68] analyzed the distribution of near-neighbor distances in LH proteins and demonstrated that the protein prevents self-quenching of (B)Chl dimers by keeping them farther apart than the critical distance. The analysis is repeated here for more recently available protein structures (Fig. 3). Clearly, the peaks of the Gaussian fit to the distributions of first plus second nearest neighbor distances are all around 10 Å center to center, which is consistent with the proposed self-quenching constraint.

The specific mechanisms by which (B)Chl dimers and higher aggregates quench fluorescence have not yet been clarified, although it is clear that at shorter distances it is more likely to find non-radiative decay pathways to the ground state at most pigment orientations. Nonetheless, self-quenching may be avoided at a few unique relative orientations even at shorter distances. This is the case in the chlorosomes of green photosynthetic bacteria in which thousands of BChl *c* pigments comprising over 99% of the total weight of the chlorosome, self-assemble with their transition dipoles in head to tail arrangement [69–72]. This unique arrangement is highly fluorescent and results in strong exciton coupling between the pigments and increase the effective oscillator strength about 10-fold compared to the monomers [70–72].

3.2. Excitation energy transfer

Efficient light activated charge separation systems such as the RC are not necessarily efficient light absorbers. Natural solar energy conversion systems separate LH and RC components, which allows for engineering and optimizing components separately and largely independently, but requires efficient coupling between the functional elements. Yet, before we describe the details of energy transfer in PSUs, it is important to note that their naturally selected architecture comprising separate LH and RC components which has been conserved throughout evolution, is not the only feasible architecture for solar energy conversion under limiting light conditions. Many non-natural photovoltaic cells operate at conversion yields that are comparable or even surpass natural photosynthetic systems but rely on direct absorption of excitation energy by densely packed electron transfer modules [73,74]. Thus, it is possible to design systems in which every light absorber is directly associated with charge separating centers, although this incurs the synthetic cost of building many extra charge separating components. Energy transfer considerations are, of course, irrelevant for these designs.

While natural PSU design critically depends on fast transfer of excitation energy within and from the light absorption unit, and on efficient trapping by the charge transfer unit, the constraints imposed by the fundamental physics of energy transfer are very permissive. With a typical (B)Chl fluorescence

Table 1
Weight percentage of chlorophylls (Chls), bacteriochlorophylls (BChls) and carotenoids

	LH2 (1NKZ)	FMO (1M50)	PCP (1PPR)	PSI (1JB0)	PSII (1S5L)	LH1–RC (1PYH)	LHCII (1RWT)
Protein	72%	86%	83%	73%	89%	86%	62%
(B)Chls	19%	14%	4%	22%	10%	14%	30%
Carotenes	10%	0%	13%	3%	1%	0%[a]	8%
Total Pigment	28%	14%	17%	25%	11%	14%	38%

Abbreviations: LH2—peripheral LH complex 2 of purple bacteria, FMO—Fenna Mathews Olson protein, PCP—peridine Chl protein, PSI—cyanobacterial photosystem I, PSII—plant photosystem II, LH1-RC—purple bacterial RC and core LH complex, LHCII—plant peripheral LH complex II.

[a] Unresolved in the crystal structure.

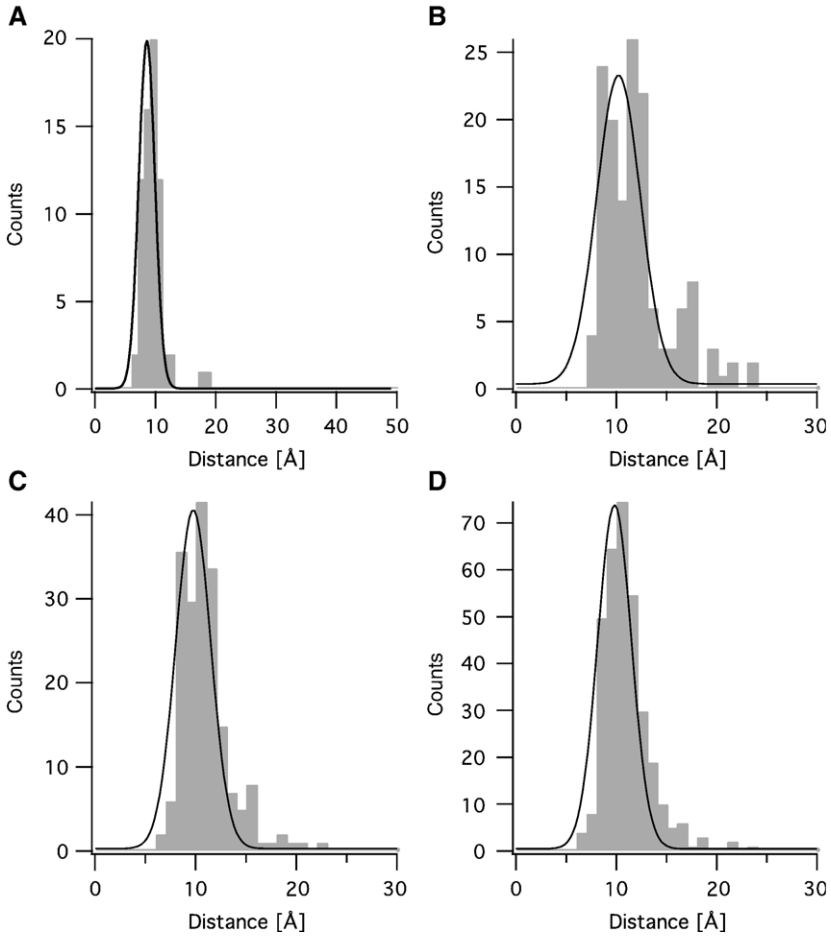

Fig. 3. Nearest and second nearest neighbor distances (grey bars) in purple bacterial LH1–RC complex (PDB: 1PYH) (A), plant photosystem II (PDB: 1S5L) (B), cyanobacterial photosystem I (PDB: 1JB0) (C), and plant PSI–LHCI complex (PDB: 1QZV) (D). Distances are measured between central Mg atoms of each (B)Chl. The centers of the Gaussian curves fitted to each distribution (solid line) are 8.59±0.04, 10.2±0.2, 9.74±0.09, and 9.82±0.05 Å, respectively, and the widths are 1.89±0.06, 3.1±0.3, 2.5±0.1 and 2.38±0.07 Å, respectively.

lifetime of 1 ns and a Förster radius (r_o) of 80 Å, [58], excitation energy is transferred efficiently over distances of several nanometers by the Förster mechanism (Fig. 2B, left), whereas light-absorption constraints typically limit nearest neighbor distances (r) to more than 10 Å (Fig. 3). This large ratio between Förster radius and absorption limited chromophore distances (r_o/r) implies that EET steps are generally not limited to nearest neighbors, which enhances connectivity between the LH pigments and provides multiple pathways for the excitation energy to rapidly reach the RC.

Fig. 4 reveals the high interconnectivity between LH (B)Chls in the distribution of pigment–pigment distances of the currently available photosystem structures. Clearly, the distribution of inter (B)Chl distances is not uniform, avoiding distances of less than 10 Å, and favoring distances between 40 and 80 Å. Strikingly, the distance between a given (B)Chl and RC pigment is mostly within 40 Å. According to Eq. (3), a 40 Å distance and a 80 Å Forster radius translates into an EET rate at least 64 fold faster than the radiative decay rate and an energy transfer quantum yield of 98.5% or more.

The highly redundant network of EET pathways from LH to RC pigments is extremely robust and increases the probability of trapping excitation energy by the RC. Recent computational studies of PSI and the core LH ensembles of PSII emphasize the robustness of their design, even without energy "funneling" and ideal orientations of pigments. Yang et al. [65] could not discern a significant energy funnel from the core LH components of PSI towards the RC and revealed only minor variations in trapping time and transfer rates upon random changes of site energies and relative pigment orientations. Similarly, Sener et al. [64], using a different computational approach, have shown only marginal fluctuations in EET quantum yield upon changing the relative dipole orientations, site energies and even pruning individual Chls from the LH ensemble. Vasil'ev and Bruce have demonstrated similar trends in PSII [63].

While computations show the effect of random changes in a single random (B)Chl has little effect on overall quantum yield, the computed yields of the native energetic configurations and dipole orientations of PSI and PSII pigments do approach 100%, well above the 90% or 96% expected for completely random orientation of all transition dipoles or random site energies [63]. This suggests a role for natural selection in increasing LH efficiency. Furthermore, some Chls that appear to

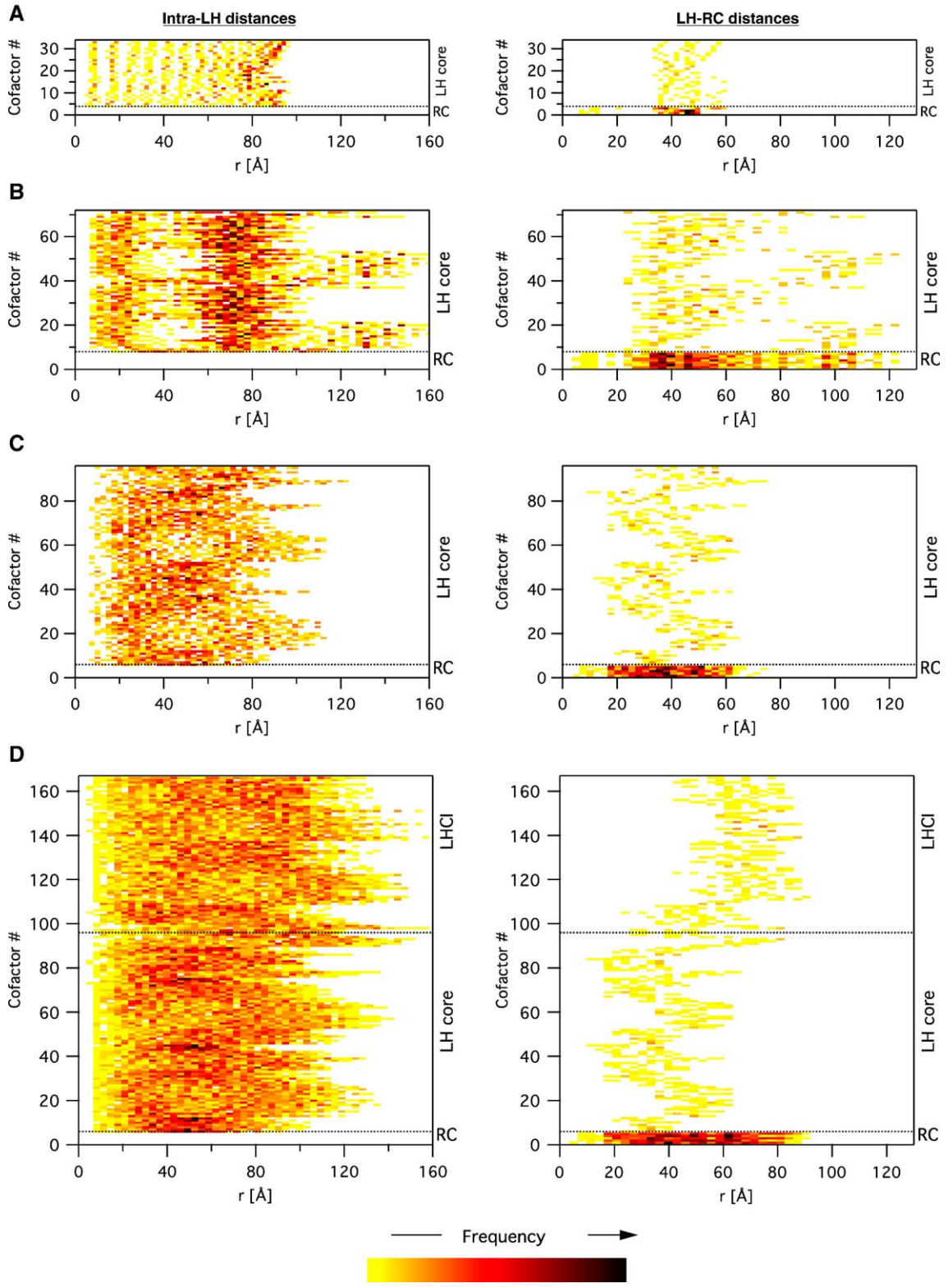

Fig. 4. Distribution of (B)Chl distances within LH pigments (left) and between LH and RC pigments (right) in purple bacterial LH1–RC complex (PDB: 1PYH) (A), plant photosystem II (PDB: 1S5L) (B), cyanobacterial photosystem I (PDB: 1JB0) (C), and plant PSI–LHCI complex (PDB: 1QZV) (D). Each row of pixels in the images represents a histogram of distances of one (B)Chl to the rest of the (B)Chls in the complex where the occurrence frequency of any distance is color scaled from yellow to red to black (uncolored pixels represent no counts).

have been conserved through the evolution of PSI and PSII do have more significant effects on quantum yield than others [63]. Although natural selection under limiting light conditions may have improved light-harvesting efficiency by a few percents, such orientation control is likely to be of marginal significance for engineering non-biological photosystems.

While the high pigment connectivity in PSU greatly enhances the chances of energy trapping by the RC, it also increases the chances of energy dissipation in the presence of other quenching centers. These may be used for protection against excessive light exposure but must be strictly controlled in order to avoid dissipative traps that will totally quench photoexcitation energy. Carotenoids, while complementing the absorption cross-section of visible light of most PSUs, are another important class of quenchers and protective molecules because of their extremely fast non-radiative decay rates and therefore very short excited state lifetimes. Achieving a strong coupling for effective energy transfer between carotenoids and (B)Chl before energy dissipation requires specific geometries. Yet, even when carotenoids are positioned at van der Waals contact and are strongly coupled to acceptor (B)Chls, energy transfer rates are at best on the same time scale of excited state relaxation with yields of 30–70% [75]. However, by manipulating and exploiting the optically forbidden but longer lived (picoseconds) S_1 excited state of the carotenoids, the LH complexes of PCP improve the carotenoid to Chl EET yield to almost 100% [76].

Cation and anion radicals are also very efficient quenchers of excitation energy [77]. The proximity of LH and RC pigments required for efficient EET increases the risk of forming such radicals by short-circuiting the energy and electron transfer units. These short-circuits due to ET between LH pigments and redox intermediates of the electron transfer chain might deactivate the LH unit because the RC electron transfer chains are designed to effectively carry away counter-charges thereby generating long-lived radicals. Deactivation may be only temporary if charge recombination takes place, yet in many cases, radicals may further react with other LH pigments, nearby protein residues, lipids, or water molecules thereby causing degradation of the LH unit. As shown in Fig. 5, the chances of permanent damage depend on relative ET rates between LH and RC pigments (e.g., reactions D1–D3), the rates of productive ET (P1–P3) and charge recombination (U1–U3). While at short LH-RC distances, charge recombination reactions (U2, U3) are fast enough to prevent permanent damage by destructive antenna reduction (D1, D4) or oxidation (D2, D5), as the electron is transferred to secondary acceptors (P2) and the highly oxidizing form of the primary donor is stabilized, antenna oxidation may immediately result in a neutral RC and a radical trap within the LH unit. Thus, the extent of permanent damage to the PSU depends primarily on the ratio of ET rate between LH pigments and the primary donor (D3) to the reoxidation rate of the latter (P3). Indeed, simple length and energy scales considerations demonstrate how natural PSUs evolved to minimize the ratio K_{D3}/K_{P3} without compromising efficiency.

Table 2 lists the midpoint potentials, E_m, of primary donors in purple bacterial, PSI, and PSII RCs, their cation radical

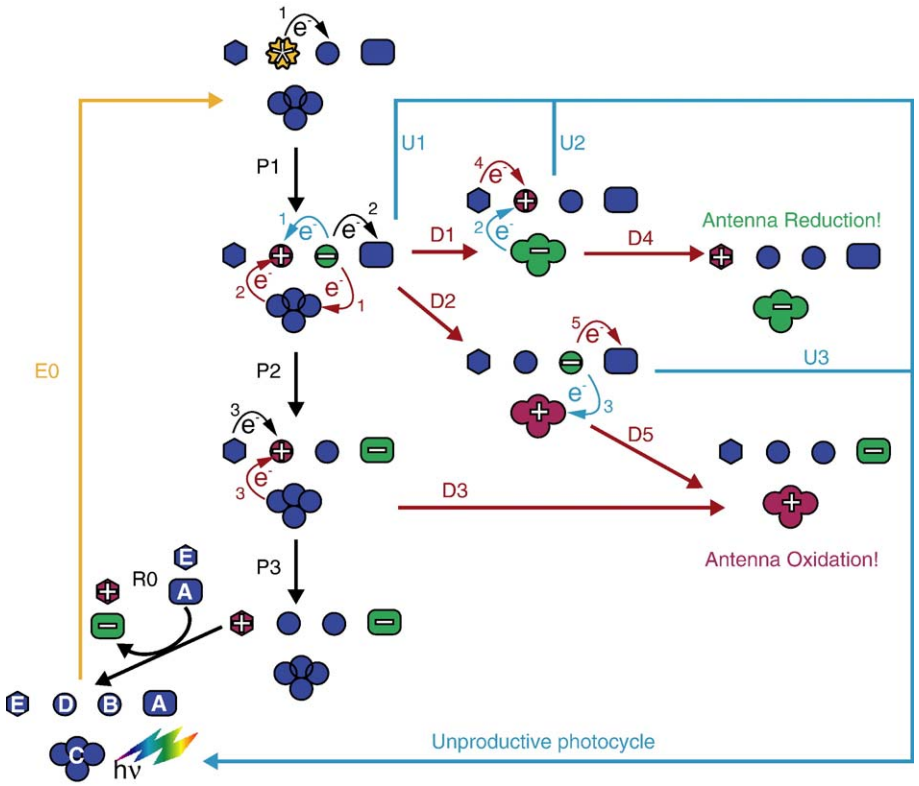

Fig. 5. Productive (black), unproductive (cyan), and destructive (red) ET reactions in a generic photosystem comprised of an antenna (C), a photoexcitable donor (D), a primary acceptor (B), and an external (replaceable) donor (E) and acceptor (A). A productive cycle is initiated by Photoexcitation (E0) of D either directly or via EET from C (not shown), followed by ET reactions P1–P3 to yield oxidized *E* and reduced A. The system is ready for the next photocycle after these are replaced by new *E* and A (R0). Charge recombination reactions U1–U3 lead to a futile photocycle but keep the system functional. In contrast, ET reactions D1–D5 result in permanent damage by reducing or oxidizing the antenna. (For interpretation of the references to colour in this figure legend, the reader is referred to the web version of this article.)

Table 2
LH–RC minimal coupling distances

		RC			LHC		
		E_m [V]	τ_{max}	A_{max}	E_m [V]	ΔG° [eV]	r_{min} [Å]
LH1–RC [80,81]	$P865^{+\cdot}$	0.50	25 μs	9%	0.57	+0.07	24
PSI [82]	$P700^{+\cdot}$	0.39	12 μs	100%	0.85[a]	+0.45	0
PSII [83,84]	$P680^{+\cdot}$	1.12	12 μs	18%	0.85[a]	−0.27	18

[a] Based on redox potentials of Chl a in organic solvents [85].

lifetimes, $\tau_{max}=1/K_{P3}$, (when the kinetics of RC primary donor reduction involves more than one phase, we consider the slowest and take into account its amplitude, A_{max}) and estimated E_m values of the respective LH components. Table 2 shows clearly that LH oxidation is not an issue in PSI because oxidation by $P700^+$ is energetically unfavorable. In contrast, LH oxidation certainly needs to be considered in PSII where LHC oxidation by $P680^+$ is favorable ($\Delta G^\circ=-0.27$ eV). In purple bacterial PSUs, LH1 oxidation is about 0.07 eV uphill yet it cannot be disregarded because electron transfer within the closely packed LH1 pigments is rapid and, considering site energy inhomogeneity, it is possible to trap the BChl cation radical in a lower potential site [78, 79]. Using Eqs. (2) and (3) with typical reorganization energy (λ) of 0.7 eV, and a typical fluorescence relaxation time (τ) of 3 ns we calculate a minimal distance, r_{min}, from each of the RCs that guarantees that the ratio of unproductive to productive rates, $K_{D3}/K_{P3}=K_{D3}\,\tau_{max}<1\%$.

Fig. 6 compares the (B)Chl organization in purple bacterial LH1–RC complex, PSI, and PSII. The pigment distances from the middle of P865, P700, and P680 are plotted in Fig. 6B, with the bacterial, PSI and PSII RC pigments enclosed by the orange, blue, and red ellipses, respectively. Adding the r_{min} values in Table 2 to the axes of these ellipses defines the predicted "cordon sanitaire" [51] represented by the shaded areas. This pigment-free zone around the RC pigments ensures that LH pigments oxidation should occur only in 1% or less of the photocycles. Evidently, the pigment arrangement in all PSUs corresponds well with the values of r_{min}. As expected, PSI antenna pigments are packed closest to the RC, some within 10 Å (edge to edge), whereas in PSII and the LH1–RC complex there are no antenna pigments within 20 and 35 Å (edge to edge) from the RC, respectively. Although the increased distance significantly slows the energy transfer rate from ~1 ps in PSI to ~100 ps and ~30 ps in PSII and purple bacterial PSU, respectively, it is conveniently fast enough for a near unity EET yield.

3.3. Charge separation

The fundamental time constraints required for electronic charge separation are more complex than for EET. Electron

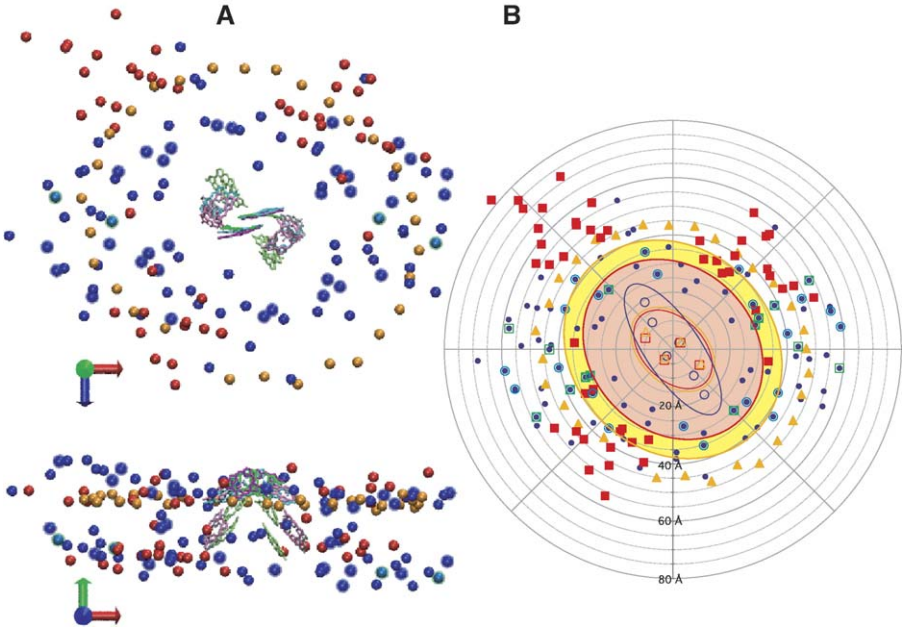

Fig. 6. (A) Comparison of Chl/BChl arrangements in LH1–RC complex (orange), PSI (blue) and PSII (red). Antenna systems are represented by the central Mg atoms of their Chls/BChls, aligned at the RC primary donor. RC pigments are shown in stick representation. Bacterial, PSI and PSII RCs are colored cyan, green, and pink, respectively. Images were created with VMD [86]. (B) A polar plot representing distance and radial distributions from the middle of the central pair of RC (B)Chls. LHC and RC components are marked by full and open symbols, respectively. The pigments of PSI, PSII, and bacterial RCs are encircled by the blue, red, and orange ellipses, respectively, whereas the calculated "cordon sanitaire" for PSII and bacterial LH1–RC are represented by the red and orange areas, respectively.

tunneling rates decay steeply exponentially with distance (Eq. (2)) and therefore, in contrast to EET, ET across a 35 Å transmembranal barrier is prohibitively slow and can be discounted. Furthermore, light-driven charge separation is initiated by an ET step from an excited state and must occur before relaxation to the ground state takes place, typically within a few nanoseconds. The charge-separated state must then be maintained up to several microseconds in order to facilitate ET to diffusive electron carriers. Nature adapts to these constraints by using the simple device of chains of redox cofactors (Fig. 1) whereby consecutive tunneling over several short steps replaces the exponentially slower tunneling rates at long distances with an approximate linear dependence of rate decrease on distance tunneled [55,56]. Indeed, electron tunneling simulations show that most of the electron transfer reactions in the photosystems and the resulting high efficiency of charge separation on seconds timescale can be understood in terms of simple tunneling limited electron transfer between closely spaced redox centers (Figs. 7 and 8).

It is apparent from Fig. 7 that the cofactor organization in the RCs of known molecular structure is similar despite their very different redox potentials and energetics (Table 3). It is these differences in energetics that are responsible for the functional differences in the RCs. The redox chlorins at the core of all RCs form an obvious chain with separations of less than 6 Å that ensure tunneling times of 10 ps or less. The effect of the common (B)Chl chain is to permit the photo-induced oxidant and reductant to reside briefly on any of the (B)Chls, subject principally to the free energy of that state and the energetic penalty of any uphill reverse electron transfer (Eq. (2)). This is clearest in PSII, where it appears that the relatively small energy gap of about 0.1 eV between the Pheophytins (Phs) and the Chls allows any electron on the electron transfer-"inactive" D2 side Ph (Ph_{D2}) to thermally equilibrate with other Chls on a rapid time scale. Nonetheless, small differences in redox potential appear to favor the accessory Chl (Chl_{D1}) adjacent to the "active" Ph (Ph_{D1}) as the primary donor [87–90]. In the purple bacterial RC, more obvious differences in redox potential make the central BChl pair act as the primary donor and to be the preferred site for the resulting cation radical 'hole'.

The fate of $P680^{\bullet+}$, the highly oxidizing hole in PSII, will be governed by the redox differences between the four chlorophylls, all of which have high redox potentials in the region of 1.2 V [88,91,92]. Since the tyrosine donors Tyr_Z and Tyr_D are oxidized at about the same rate [93] and are more or less equidistant from the P_A and P_B Chls, respectively (see Fig. 3), then on the first photochemical turnover the hole must be delocalized more or less equally between the two Chls P_A and P_B even at low temperatures. This symmetry in electron donation is broken by the fact that the Mn cluster which

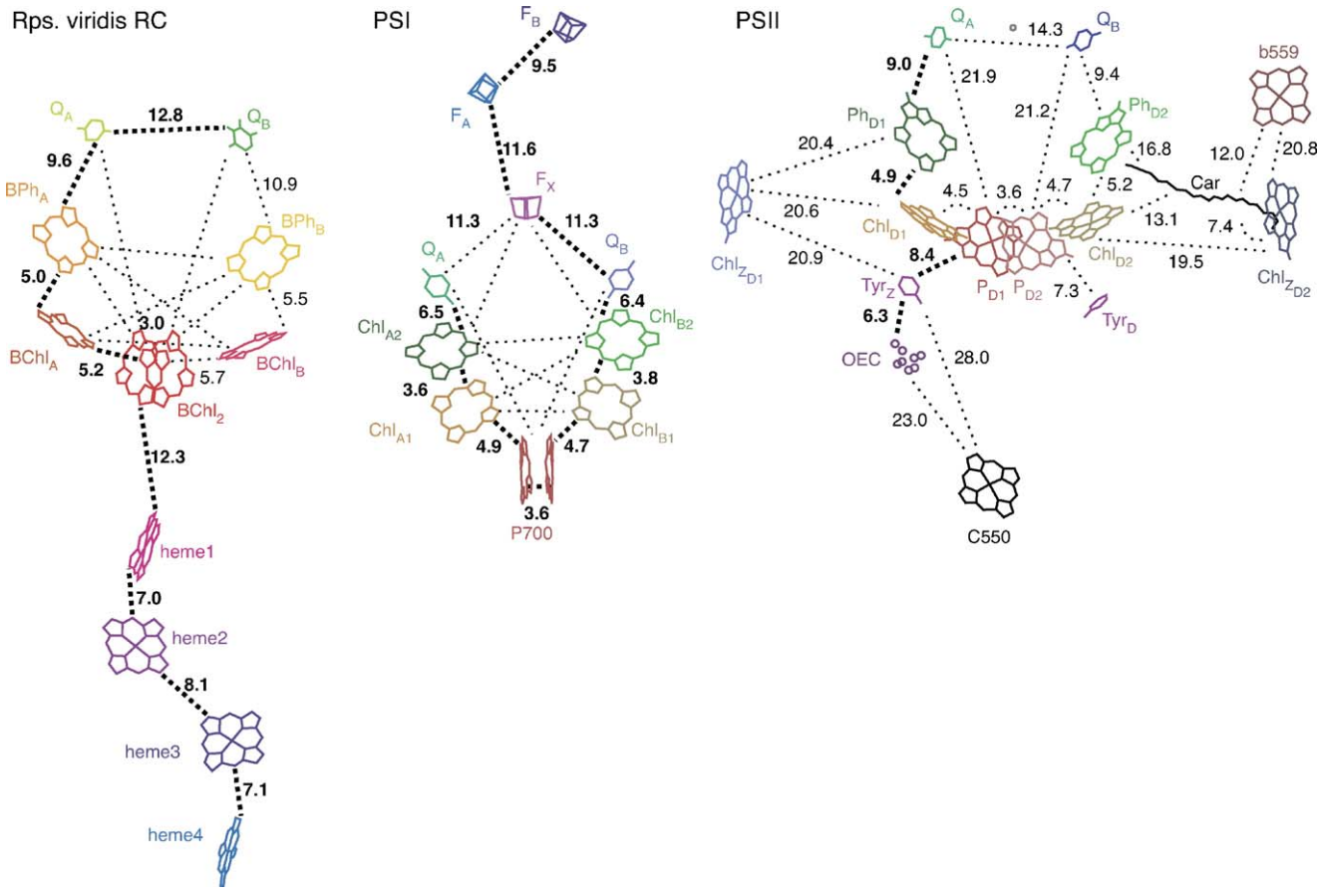

Fig. 7. The arrangement of cofactors in the structure of cyanobacterial reaction centers PSI (PDB: 1JB0) and PSII (PDB: 1FE1) from *Syn. elongatus*, and purple sulfur bacterial reaction center (PDB: 1PCR) from *Rps. viridis*). Bold lines and numbers refer to edge-to-edge distances in likely productive electron transfer reactions. Other distances reflect possible electron-tunneling reactions considered in simulations, and that may be revealed under certain experimental conditions.

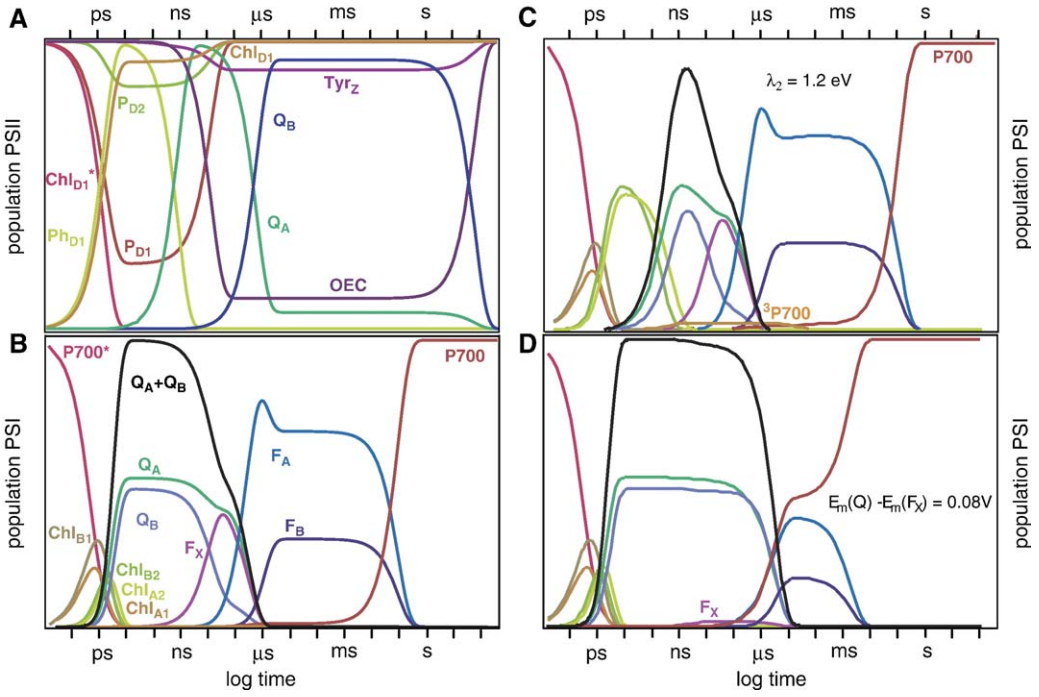

Fig. 8. Individual redox components rise and fall in their state of reduction in electron tunneling simulations of PSI and PSII. The left panels show simulations of PSII and PSI (A and B, respectively) using distances of Fig. 7 and redox properties of Table 3 combined with reorganization energies similar to purple bacterial RC: 0.3 eV between reduced or neutral Chls or Phs (λ_1), 0.3 eV between reduced or neutral Chl and quinone (λ_2) [122], 0.6 eV between quinone and Chl cations (λ_3), 0.85 between quinones and FeS (λ_4), 1 eV between FeS and Chl cation (λ_5), and 1.1 eV between FeS centers (λ_6) [97]. A system of differential equation connects all redox centers with tunneling rates calculated using equation 2. The right panels show the robustness of charge separation in PSI when changing λ_2 from an optimal value of 0.3 eV to 1.2 eV (C), but sensitivity to positive drift in the E_m of Q (D).

catalyses the water oxidation process, is located only on the D1 side. The consequences of this is that the P_A Chl becomes the active $P680^{\bullet+}$ species, presumably because the long lived inactive Tyr_D radical cation generated during the first or second photochemical turnover increases the redox potential of P_B relative to P_A. Direct evidence that P_A does indeed generate the $P680^{\bullet+}$ species has come from recent mutational studies [88]. The electron transfer from Tyr_Z to P_A may, in part be coupled to proton release from the tyrosine which could then facilitate an electron/proton abstraction from the substrate water molecules

Table 3
Estimated redox midpoint potentials in photosystems

Rps. viridis RC		PSI		PSII	
Cofactor[a]	E_m	Cofactor[a]	E_m	Cofactor[a]	E_m
$BChl_2$	0.50 [101]	P700	0.45 [102]	Chl_{D1}	1.26 [91]
$BChl_2^*$	−0.79	P700*	−1.17 [103]	Chl_{D1}^*	−0.57 [91]
$BChl_A$	−0.71	^{3}P700	−0.82[104]	P_{D1}	1.20 [88]
$BChl_B$	−0.85	Chl_{1A}	−1.29 [97]	P_{D2}	1.24 [88]
BPh_A	−0.63 [105]	Chl_{1B}	−1.29 [97]	Chl_{D2}	1.26 [92]
BPh_B	−0.63	Chl_{2A}	−1.05 [106]	Ph_{D1}	−0.39 [91]
Q_A	−0.15 [107]	Chl_{2B}	−1.05 [106]	Ph_{D2}	−0.39 [92]
Q_B	0.04 [108]	Q_A	−0.70 [97]	Q_A (w/o OEC)	−0.03 (0.065) [109, 110]
Heme 1	0.38 [111]	Q_B	−0.74[112]	Q_B	0.04 [113]
Heme 2	0.02 [111]	F_X	−0.67 [114]	Tyr_Z (w/o OEC)	1.075 (~0.95) [91]
Heme 3	0.32 [111]	F_A	−0.54 [97]	Tyr_D	0.75 [115]
Heme 4	−0.06 [111]	F_B	−0.56 [97]	OEC-Mn S1/S2	1.02 [91]
				$^3(P^+Ph^-)$	−0.42 [91]
				carotenoid	~1.06 in micelles (~0.927 calc) [116]
				b559 (w/o OEC)	0.35 (0–0.08) [117, 118]
				Chl_{ZD2}	0.916 [119]
				Chl_{ZD1}	0.920 [119]
				c550	−0.08 [120]

[a] See Fig. 7.

bound to the Mn cluster [94]. It is the involvement of bond-making/breaking proton transfer at the tyrosines and the Mn cluster that makes it likely that these electron transfer reactions are not strictly tunneling limited.

The structural symmetry of the (B)Chls in the RC means that there are two branches of the (B)Chl chain that form the start of the cofactor chain extending across the membrane. In the case of PSI and even more so in the RC of green sulfur bacteria [95], there may also be a near functional symmetry of electron transfer across these chains to the symmetrically placed quinone acceptors and then to the centrally located iron–sulfur center, F_x [17,89,96,97]. However, in the case of RCs of purple bacteria and PSII the situation is quite different. Only one of the quinones (Q_A) appears to be designed as the functional acceptor from the A branch BChls/bacteriopheophytins (BPhs) in purple bacterial RC or Chl/ Ph in PSII. How is the high quantum efficiency of charge separation maintained by guiding electron transfer down the appropriate A branch of these RCs? In the case of the purple bacterial RC, if the energy gap between the BPhs and the BChls on both branches are about 0.16 eV, then some electrons could be trapped on the inactive BPhs leading to energy wasting charge recombination to the BChl dimer ground state. Indeed, under certain experimental conditions (e.g., excess light), the B side BPh can be driven reduced [98]. The active A side BPh (BPh_A) may be favored kinetically, rather than thermodynamically, by a lower B side BChl ($BChl_B$) monomer redox potential that makes electron transfer from the dimer to this side sufficiently uphill; a similar effect can be accomplished by a larger reorganization energy for this electron transfer [99, 100].

Although the redox energetic differences between the photosystems contribute to their functional differences, this does not mean that the energetic parameters are precisely "tuned" and optimized. Rather, the closely spaced organization of cofactors leads to high engineering tolerance with regard to energetic parameters. Increasing numbers of electron transfer chains are being uncovered that include energetically unfavorable redox steps and yet promote net rapid ET rates in an overall favorable downhill process. Endergonic ET through intermediates hundreds of meV uphill can take place faster than typical enzymatic turnover times provided the redox centers are closer than 14 Å. The smaller the distance, the more energetically unfavorable the electron transfer intermediate can be. The heme chain in *Rps. viridis*, which extends from the $BChl_2$ out into the periplasm some 60–70 Å to a docking site for soluble cytochrome c_2 at the terminus (Fig. 7), is an archetypical example. The chain is characterized by close, 7–8 Å positioning of the hemes and intrinsically poised to promote very rapid tunneling. The reduction potentials describe a dramatic sequence of several hundred millivolts endergonic and exergonic tunneling steps that overall, from the cytochrome c_2 to the $BChl_2$, is modestly exergonic [111,121].

The RC of PSI is another example whereby simple distance between the various cofactors contributes to a collective robustness of function that apparently has not undergone much fine-tuning of the energetic and packing parameters that influence electron tunneling rates. This robustness can be demonstrated by simulating electron tunneling kinetics and varying energetic parameters in Eq. (2) (Fig. 8). Simulations beginning with photoexcited state Chl^*_{D1} show that even without including the stabilizing effect of electron transfer to $P700^+$ from the external donor, plastocyanin, the architecture of PSI favors a high yield of light induced charge separation over wasteful charge recombination. As an example of tolerance, the reorganization energy of the Chl to quinone electron transfer can range from optimal values near 0.3 eV to a value as large as 1.2 eV before charge recombination through the formation of triplet state $^3P700$ begins to be a problem (Fig. 8C).

Robustness is also seen in substitutions [122] with other quinonoid molecules of the native Q_A or Q_B phylloquinones that drop the redox midpoint from the native −0.74 to −0.70 V to as low as −1 V before the electron begins to be shared significantly between the quinones and the Chls. There is a limit, however, on how far the redox potential of Q_A/Q_B can be

Table 4
Engineering guidelines for PSU design

Process	Constraint	Guideline[a]
Light absorption	Incoming photon flux is rate limiting	Increase absorption cross section by using dense arrays of pigments Use multiple chromophores with complementary absorption spectra that match the spectral distribution of incoming photons *Expand the useful spectral range by utilizing lower energy photons. This requires lowering the driving force of the charge separation reaction.*
EET	Excitation energy should be trapped by the RC	Interconnect several cofactors to allow multiple EET pathways within LH pigments and between LH and RC. *Adjust site energies of cofactors to form an energy funnel from the periphery to the RC*
EET	Strongly coupled dimers may become non-radiative, unproductive traps	Avoid placing pigments within less than 10 Å from each other *Restrict relative orientations of pigments such that EET is preferred over non-radiative decay*
EET	ET to/from the RC may create harmful radicals in the LH unit	Form a "cordon sanitaire" around the RC beyond which ET rates to/from RC are marginal compared to EET rates
ET	Single step electron tunneling across transmembranal distances is prohibitively slow	Use chain of redox cofactors spaced within 14 Å (edge to edge) from each other
ET	ET from the excited state competes with relaxation to the ground state	Place acceptor within 5 Å from the photoexcited donor

[a] Guidelines in italics improve yield but are not critical.

raised above the E_m of F_x because the electron will tend to remain on Q_A or Q_B long enough for wasteful direct charge recombination to the ground state to become a problem (Fig. 8D). With a relatively broad tolerance of E_m ranges of the quinones Q_A and Q_B, it may be fair to say that the observed asymmetry in the electron transfer kinetics of the two branches does not reflect an advantageous design feature of PSI, but merely a tolerable evolutionary drift that has little effect on performance. Perhaps more surprising is the low redox potential value of F_x since this forces the design of a quinone binding site to keep the midpoint potential of the quinone at an unusually low value below about −0.70 V. Certainly, the system could tolerate a rise of 0.1 V in the F_x midpoint potential and still keep the electrons on F_a and F_b, ready for subsequent reduction of ferredoxin. The present redox properties of F_x may represent the adoption of a "good enough" electron transfer system, in which the position of the F_x on the symmetry axis of PSI with good proximity to Q_A, Q_B and F_a secures the single most important parameter in determining the electron tunneling rates.

4. Applying natural photosystem engineering guidelines for custom-building molecular photovoltaic devices

We conclude by briefly contemplating construction of custom-built PSUs according to the engineering guidelines that emerge from our examination of the natural systems. These are summarized in Table 4 and reveal that the physical and chemical principles of light absorption, EET, and ET processes dictate the use of multiple cofactors in densely packed LH arrays and in closely spaced redox chains for increased absorption cross section and ET range, respectively. The fundamental time, energy and length scales of these processes allow for a high degree of flexibility in PSU design and engineering, yet, the key for successful application is controlling intercofactor distances with sub-nanometer accuracy. In an electron transfer chain, for example, increasing the distance between two cofactors in an average protein medium by 0.5 nm will elicit a 1000 fold decrease in electron transfer rate, and placing two Chls within the same distance in a LH array might introduce a non-radiative trap that will compete with productive EET to the RC. Gaining such precise control over molecular assemblies of nanoscale dimensions is a great challenge and the focus of intensive research by many scientific disciplines [123–129].

Using de novo designed proteins for constructing efficient molecular photoconversion devices is an appealing and promising method with many unique possibilities including inexpensive production through expression in bacterial systems, high yield and high purity as well as considerable versatility and adaptability to various construction requirements and external conditions. However, designing proteins that can bind and organize cofactors up to 20% of their total weight is still too complicated problem to be addressed by protein de novo design. This is mainly because of the multiple possibilities and many degrees of freedom involved in cofactor–protein interactions [127,130] and practical issues regarding cofactor self-aggregation. Furthermore, because we expect membranes or, alternatively, air–water interfaces, solid surfaces or nanoporous materials, to provide templates for organizing the protein-based devices and to provide the dielectric barriers to support the desired macroscopic function, new designs adjusted for self-assembly in these environments are being developed.

Unfortunately, our understanding of the principles that underlie structure and folding of this type of proteins lag significantly behind our understanding of water-soluble proteins [125,126]. Nevertheless, progress is being made; modular amphiphilic designs of four-helix bundles comprised of a water-soluble protein domain continuous with a lipophilic membrane associated domain have been successfully assembled [131–136] along with specific ligation to hemes and BChl derivatives in the lipophyllic and hydrophyllic domains.

Although there is much work to do, with continued progress in understanding how to balance the interactions that guide protein folding and assembly within membranal environments and the packing of organic cofactors within a protein core, design and engineering of efficient PSUs based on de novo designed proteins should be feasible.

Acknowledgements

The authors acknowledge financial support from NIH grant GM41048 and NSF grant DMR00-79909 to PLD, and Human frontiers science program organization long term fellowship to DN.

References

[1] H. Gest, R.E. Blankenship, Time line of discoveries: anoxygenic bacterial photosynthesis, Photosynth. Res. 80 (2004) 59–70.
[2] Govindjee, D. Krogmann, Discoveries in oxygenic photosynthesis (1727–2003): a perspective, Photosynth. Res. 80 (2004) 15–57.
[3] R. Emerson, W. Arnold, The photochemical reaction in photosynthesis, J. Gen. Physiol. 16 (1932) 191–205.
[4] R. Emerson, W. Arnold, A separation of the reactions in photosynthesis by means of intermittent light, J. Gen. Physiol. 15 (1932) 391–420.
[5] H. Gaffron, K. Wohl, The theory of assimilation, Naturwissenschaften 24 (1936) 166–167.
[6] L.N.M. Duysens, Transfer of Excitation Energy in Photosynthesis, State University, Uterecht, The Netherlands, 1952.
[7] R.K. Clayton, W. Arnold, Absorption spectra of bacterial chromatophores at temperatures from 300 degrees K to 1 degree K, Biochim. Biophys. Acta 48 (1961) 319–323.
[8] B. Chance, M. Nishimura, On the mechanism of chlorophyll–cytochrome interaction: the temperature insensitivity of light-induced cytochrome oxidation in chromatium, Proc. Natl. Acad. Sci. U. S. A. (1960) 19–25.
[9] D. DeVault, B. Chance, Studies of photosynthesis using a pulsed laser: I. Temperature dependence of cytochrome oxidation rate in chromatium. Evidence for tunneling, Biophys. J. 6 (1966) 825–847.
[10] J. Deisenhofer, O. Epp, K. Miki, R. Huber, H. Michel, Structure of the protein subunits in the photosynthetic reaction center of rhodopseudomonas-viridis at 3Å resolution, Nature 318 (1985) 618–624.
[11] M.Z. Papiz, S.M. Prince, T. Howard, R.J. Cogdell, N.W. Isaacs, The structure and thermal motion of the B800–850 LH2 complex from Rps. acidophila at 2.0 Å resolution and 100 °K: new structural features and functionally relevant motions, J. Mol. Biol. 326 (2003) 1523–1538.
[12] G. McDermott, S.M. Prince, A.A. Freer, A.M. Hawthornthwaite-Lawless, M.Z. Papiz, R.J. Cogdell, N.W. Isaacs, Crystal-structure of an integral membrane light-harvesting complex from photosynthetic bacteria, Nature 374 (1995) 517–521.

[13] J. Koepke, X.C. Hu, C. Muenke, K. Schulten, H. Michel, The crystal structure of the light-harvesting complex II (B800–850) from *Rhodospirillum molischianum*, Structure 4 (1996) 581–597.
[14] K. McLuskey, S.M. Prince, R.J. Cogdell, N.W. Isaacs, The crystallographic structure of the B800–820 LH3 light-harvesting complex from the purple bacteria *Rhodopseudomonas acidophila* strain 7050, Biochemistry 40 (2001) 8783–8789.
[15] Z.F. Liu, H.C. Yan, K.B. Wang, T.Y. Kuang, J.P. Zhang, L.L. Gui, X.M. An, W.R. Chang, Crystal structure of spinach major light-harvesting complex at 2.72 angstrom resolution, Nature 428 (2004) 287–292.
[16] A. Zouni, H.T. Witt, J. Kern, P. Fromme, N. Krauss, W. Saenger, P. Orth, Crystal structure of photosystem II from *Synechococcus elongatus* at 3.8 angstrom resolution, Nature 409 (2001) 739–743.
[17] P. Jordan, P. Fromme, H.T. Witt, O. Klukas, W. Saenger, N. Krauss, Three-dimensional structure of cyanobacterial photosystem I at 2.5 angstrom resolution, Nature 411 (2001) 909–917.
[18] K.N. Ferreira, T.M. Iverson, K. Maghlaoui, J. Barber, S. Iwata, Architecture of the photosynthetic oxygen-evolving center, Science 303 (2004) 1831–1838.
[19] N. Kamiya, J.R. Shen, Crystal structure of oxygen-evolving photosystem II from *Thermosynechococcus vulcanus* at 3.7-angstrom resolution, Proc. Natl. Acad. Sci. U. S. A. 100 (2003) 98–103.
[20] A.W. Roszak, T.D. Howard, J. Southall, A.T. Gardiner, C.J. Law, N.W. Isaacs, R.J. Cogdell, Crystal structure of the RC-LH1 core complex from *Rhodopseudomonas palustris*, Science 302 (2003) 1969–1972.
[21] A. Ben-Shem, F. Frolow, N. Nelson, Crystal structure of plant photosystem I, Nature 426 (2003) 630–635.
[22] A. Camara-Artigas, J.P. Allen, Comparative analyses of three-dimensional models of bacterial reaction centers, Photosynth. Res. 81 (2004) 227–237.
[23] D. Stroebel, Y. Choquet, J.L. Popot, D. Picot, An atypical haem in the cytochrome b6f complex, Nature 426 (2003) 413–418.
[24] S. Iwata, J.W. Lee, K. Okada, J.K. Lee, M. Iwata, B. Rasmussen, T.A. Link, S. Ramaswamy, B.K. Jap, Complete structure of the 11-subunit bovine mitochondrial cytochrome bc_1 complex, Science 281 (1998) 64–71.
[25] C. Lange, C. Hunte, Crystal structure of the yeast cytochrome bc1 complex with its bound substrate cytochrome *c*, Proc. Natl. Acad. Sci. U. S. A. 99 (2002) 2800–2805.
[26] G. Kurisu, H.M. Zhang, J.L. Smith, W.A. Cramer, Structure of the cytochrome b_6f complex of oxygenic photosynthesis: tuning the cavity, Science 302 (2003) 1009–1014.
[27] J.H. Golbeck, The binding of cofactors to photosystem I analyzed by spectroscopic and mutagenic methods, Annu. Rev. Biophys. Biomol. Struct. 32 (2003) 237–256.
[28] P. Braun, J.D. Olsen, B. Strohmann, C.N. Hunter, H. Scheer, Assembly of light-harvesting bacteriochlorophyll in a model transmembrane helix in its natural environment, J. Mol. Biol. 318 (2002) 1085–1095.
[29] J.P. Allen, J.C. Williams, Relationship between the oxidation potential of the bacteriochlorophyll dimer and electron-transfer in photosynthetic reaction centers, J. Bioenerg. Biomembr. 27 (1995) 275–283.
[30] Z. Katiliene, E. Katilius, N.W. Woodbury, Energy trapping and detrapping in reaction center mutants from *Rhodobacter sphaeroides*, Biophys. J. 84 (2003) 3240–3251.
[31] T.M. Bricker, C. Putnam-Evans, J.T. Wu, Directed mutagenesis in photosystem II: Analysis of the CP 47 protein, Photosynth. Mol. Biol. Energy Capture, vol. 297, 1998, pp. 320–337.
[32] A. Zehetner, H. Scheer, P. Siffel, F. Vacha, Photosystem II reaction center with altered pigment-composition: reconstitution of a complex containing five chlorophyll a per two pheophytin a with modified chlorophylls, Biochim. Biophys. Acta 1556 (2002) 21–28.
[33] S. Sporlein, W. Zinth, M. Meyer, H. Scheer, J. Wachtveitl, Primary electron transfer in modified bacterial reaction centers: optimization of the first events in photosynthesis, Chem. Phys. Lett. 322 (2000) 454–464.
[34] J.L. Herek, N.J. Fraser, T. Pullerits, P. Martinsson, T. Polivka, H. Scheer, R.J. Cogdell, V. Sundstrom, B800→B850 energy transfer mechanism in bacterial LH2 complexes investigated by B800 pigment exchange, Biophys. J. 78 (2000) 2590–2596.
[35] B. Gall, A. Zehetner, A. Scherz, H. Scheer, Modification of pigment composition in the isolated reaction center of photosystem II, Febs. Lett. 434 (1998) 88–92.
[36] A. Angerhofer, F. Bornhauser, V. Aust, G. Hartwich, H. Scheer, Triplet energy transfer in bacterial photosynthetic reaction centres, Biochim. Biophys. Acta 1365 (1998) 404–420.
[37] H.A. Frank, V. Chynwat, G. Hartwich, M. Meyer, I. Katheder, H. Scheer, Carotenoid triplet-state formation in rhodobacter-sphaeroides R-26 reaction centers exchanged with modified bacteriochlorophyll pigments and reconstituted with spheroidene, Photosynth. Res. 37 (1993) 193–203.
[38] H. Savage, M. Cyrklaff, G. Montoya, W. Kuhlbrandt, I. Sinning, Two-dimensional structure of light harvesting complex II (LHII) from the purple bacterium *Rhodovulum sulfidophilum* and comparison with LHII from *Rhodopseudomonas acidophila*, Structure 4 (1996) 243–252.
[39] J.L. Ranck, T. Ruiz, G. Pehau-Arnaudet, B. Arnoux, F. Reiss-Husson, Two-dimensional structure of the native light-harvesting complex LH2 from *Rubrivivax gelatinosus* and of a truncated form, Biochim. Biophys. Acta 1506 (2001) 67–78.
[40] H. Stahlberg, J. Dubochet, H. Vogel, R. Ghosh, Are the light-harvesting I complexes from *Rhodospirillum rubrum* arranged around the reaction centre in a square geometry? J. Mol. Biol. 282 (1998) 819–831.
[41] H. Stahlberg, J. Dubochet, H. Vogel, R. Ghosh, The reaction centre of the photounit of *Rhodospirillum rubrum* is anchored to the light-harvesting complex with four-fold rotational disorder, Photosynth. Res. 55 (1998) 363–368.
[42] T. Walz, S.J. Jamieson, C.M. Bowers, P.A. Bullough, C.N. Hunter, Projection structures of three photosynthetic complexes from *Rhodobacter sphaeroides*: LH2 at 6 angstrom LH1 and RC-LH1 at 25 angstrom, J. Mol. Biol. 282 (1998) 833–845.
[43] C. Jungas, J.L. Ranck, J.L. Rigaud, P. Joliot, A. Vermeglio, Supramolecular organization of the photosynthetic apparatus of *Rhodobacter sphaeroides*, EMBO J. 18 (1999) 534–542.
[44] T.S. Bibby, J. Nield, M. Chen, A.W. Larkum, J. Barber, Structure of a photosystem II supercomplex isolated from *Prochloron didemni* retaining its chlorophyll a/b light-harvesting system, Proc. Natl. Acad. Sci. U. S. A. 100 (2003) 9050–9054.
[45] S. Scheuring, J. Seguin, S. Marco, D. Levy, C. Breyton, B. Robert, J.L. Rigaud, AFM characterization of tilt and intrinsic flexibility of *Rhodobacter sphaeroides* light harvesting complex 2 (LH2), J. Mol. Biol. 325 (2003) 569–580.
[46] S. Scheuring, J. Seguin, S. Marco, D. Levy, B. Robert, J.L. Rigaud, Nanodissection and high-resolution imaging of the *Rhodopseudomonas viridis* photosynthetic core complex in native membranes by AFM, Proc. Natl. Acad. Sci. U. S. A. 100 (2003) 1690–1693.
[47] H.W. Remigy, G. Hauska, S.A. Muller, G. Tsiotis, The reaction centre from green sulphur bacteria: progress towards structural elucidation, Photosynth. Res. 71 (2002) 91–98.
[48] J. Nield, E.P. Morris, T.S. Bibby, J. Barber, Structural analysis of the photosystem I supercomplex of cyanobacteria induced by iron deficiency, Biochemistry 42 (2003) 3180–3188.
[49] S. Bahatyrova, R.N. Frese, C.A. Siebert, J.D. Olsen, K.O. van der Werf, R. van Grondelle, R.A. Niederman, P.A. Bullough, C. Otto, C.N. Hunter, The native architecture of a photosynthetic membrane, Nature 430 (2004) 1058–1062.
[50] C.C. Moser, C.C. Page, R. Farid, P.L. Dutton, Biological electron-transfer, J. Bioenerg. Biomembr. 27 (1995) 263–274.
[51] C.C. Moser, C.C. Page, R.J. Cogdell, J. Barber, C.A. Wraight, P.L. Dutton, Length, time, and energy scales of photosystems, Adv. Protein Chem. 63 (2003) 71–109.
[52] N.J. Turro, Modern Molecular Photochemistry, University Science Books, Sausalito, CA, 1991.
[53] ASTM international, ASTM G173-03, Standard Tables for Reference Solar Spectral Irradiances: Direct Normal and Hemispherical on 37° Tilted Surface, Available at http://rredc.nrel.gov/solar/spectra/am1.5/.
[54] J. Lavergne, P. Joliot, Dissipation in bioenergetic electron transfer chains, Photosynth. Res. 48 (1996) 127–138.
[55] C.C. Page, C.C. Moser, X.X. Chen, P.L. Dutton, Natural engineering

principles of electron tunneling in biological oxidation-reduction, Nature 402 (1999) 47–52.
[56] C.C. Moser, J.M. Keske, K. Warncke, R.S. Farid, P.L. Dutton, Nature of biological electron-transfer, Nature 355 (1992) 796–802.
[57] R.C. Prince, P.L. Dutton, Single and multiple turnover reactions in the ubiquinone-cytochrome b-c2 oxidoreductase of *Rhodopseudomonas sphaeroids*: the physical chemistry of the major electron donor to cytochrome *c*2, and its coupled reactions, Biochim. Biophys. Acta 462 (1977) 731–747.
[58] R. van Grondelle, Excitation-energy transfer, trapping and annihilation in photosynthetic systems, Biochim. Biophys. Acta 811 (1985) 147–195.
[59] R. van Grondelle, J.P. Dekker, T. Gillbro, V. Sundstrom, Energy-transfer and trapping in photosynthesis, Biochim. Biophys. Acta 1187 (1994) 1–65.
[60] G.D. Scholes, Designing light-harvesting antenna systems based on superradiant molecular aggregates, Chem. Phys. 275 (2002) 373–386.
[61] G.D. Scholes, Long-range resonance energy transfer in molecular systems, Annu. Rev. Phys. Chem. 54 (2003) 57–87.
[62] T. Brixner, J. Stenger, H.M. Vaswani, M. Cho, R.E. Blankenship, G.R. Fleming, Two-dimensional spectroscopy of electronic couplings in photosynthesis, Nature 434 (2005) 625–628.
[63] S. Vasil'ev, D. Bruce, Optimization and evolution of light harvesting in photosynthesis: the role of antenna chlorophyll conserved between photosystem II and photosystem I, Plant Cell 16 (2004) 3059–3068.
[64] M.K. Sener, D.Y. Lu, T. Ritz, S. Park, P. Fromme, K. Schulten, Robustness and optimality of light harvesting in cyanobacterial photosystem I, J. Phys. Chem., B 106 (2002) 7948–7960.
[65] M. Yang, A. Damjanovic, H.M. Vaswani, G.R. Fleming, Energy transfer in photosystem I of cyanobacteria *Synechococcus elongatus*: model study with structure-based semi-empirical Hamiltonian and experimental spectral density, Biophys. J. 85 (2003) 140–158.
[66] G.S. Beddard, G. Porter, Concentration quenching in chlorophyll, Nature 260 (1976) 366–367.
[67] R.S. Knox, Spectral effects of exciton splitting in statistical pairs, J. Phys. Chem. 98 (1994) 7270–7273.
[68] G.S. Beddard, Excitations and excitons in photosystem I, Philos. Trans. R. Soc., A 356 (1998) 421–448.
[69] G.A. Montano, B.P. Bowen, J.T. LaBelle, N.W. Woodbury, V.B. Pizziconi, R.E. Blankenship, Characterization of Chlorobium tepidum chlorosomes: a calculation of bacteriochlorophyll c per chlorosome and oligomer modeling, Biophys. J. 85 (2003) 2560–2565.
[70] V.I. Prokhorenko, D.B. Steensgaard, A.R. Holzwarth, Exciton theory for supramolecular chlorosomal aggregates: 1. Aggregate size dependence of the linear spectra, Biophys. J. 85 (2003) 3173–3186.
[71] V.I. Prokhorenko, D.B. Steensgaard, A.F. Holzwarth, Exciton dynamics in the chlorosomal antennae of the green bacteria *Chloroflexus aurantiacus* and *Chlorobium tepidum*, Biophys. J. 79 (2000) 2105–2120.
[72] J. Psencik, Y.Z. Ma, J.B. Arellano, J. Hala, T. Gillbro, Excitation energy transfer dynamics and excited-state structure in chlorosomes of *Chlorobium phaeobacteroides*, Biophys. J. 84 (2003) 1161–1179.
[73] T. Markvart, Light harvesting for quantum solar energy conversion, Prog. Quantum Electron. 24 (2000) 107–186.
[74] A. Goetzberger, C. Hebling, H.W. Schock, Photovoltaic materials, history, status and outlook, Mater. Sci. Eng., R 40 (2003) 1–46.
[75] X.C. Hu, T. Ritz, A. Damjanovic, F. Autenrieth, K. Schulten, Photosynthetic apparatus of purple bacteria, Q. Rev. Biophys. 35 (2002) 1–62.
[76] A. Damjanovic, T. Ritz, K. Schulten, Excitation transfer in the peridinin-chlorophyll-protein of *Amphidinium carterae*, Biophys. J. 79 (2000) 1695–1705.
[77] C.J. Law, R.J. Cogdell, The effect of chemical oxidation on the fluorescence of the LH1 (B880) complex from the purple bacterium *Rhodobium marimum*, FEBS Lett. 432 (1998) 27–30.
[78] N. Srivatsan, D. Kolbasov, N. Ponomarenko, S. Weber, A.E. Ostafin, J.R. Norris, Cryogenic charge transport in oxidized purple bacterial light-harvesting 1 complexes, J. Phys. Chem., B 107 (2003) 7867–7876.
[79] N. Srivatsan, S. Weber, D. Kolbasov, J.R. Norris, Exploring charge migration in light-harvesting complexes using electron paramagnetic resonance line narrowing, J. Phys. Chem., B 107 (2003) 2127–2138.
[80] T.N. Kropacheva, A.J. Hoff, Electrochemical oxidation of bacteriochlorophyll a in reaction centers and antenna complexes of photosynthetic bacteria, J. Phys. Chem., B 105 (2001) 5536–5545.
[81] J.W. Farchaus, J. Wachtveitl, P. Mathis, D. Oesterhelt, Tyrosine-162 of the photosynthetic reaction-center L-subunit plays a critical role in the cytochrome-C(2) mediated reduction of the photooxidized bacteriochlorophyll dimer in rhodobacter-sphaeroides: 1. Site-directed mutagenesis and initial characterization, Biochemistry 32 (1993) 10885–10893.
[82] H. Bottin, P. Mathis, Interaction of plastocyanin with the photosystem-I reaction center—A kinetic-study by flash absorption-spectroscopy, Biochemistry 24 (1985) 6453–6460.
[83] V.V. Klimov, Discovery of pheophytin function in the photosynthetic energy conversion as the primary electron acceptor of Photosystem II, Photosynth. Res. 76 (2003) 247–253.
[84] C. Jeans, M.J. Schilstra, D.R. Klug, The temperature dependence of P680 + reduction in oxygen-evolving photosystem, Biochemistry 41 (2002) 5015–5023.
[85] T. Watanabe, Electrochemistry of chlorophylls, in: H. Scheer (Ed.), Chlorophylls, CRC Press, Boca Raton, FL, 1991, pp. 287–315.
[86] W. Humphrey, A. Dalke, K. Schulten, VMD: visual molecular dynamics, J. Mol. Graph. 14 (1996) 33–38.
[87] J.P. Dekker, R. Van Grondelle, Primary charge separation in Photosystem II, Photosynth. Res. 63 (2000) 195–208.
[88] B.A. Diner, E. Schlodder, P.J. Nixon, W.J. Coleman, F. Rappaport, J. Lavergne, W.F.J. Vermaas, D.A. Chisholm, Site-directed mutations at D1-His198 and D2-His 97 of photosystem II in synechocystis PCC 6803: sites of primary charge separation and cation and triplet stabilization, Biochemistry 40 (2001) 9265–9281.
[89] J. Barber, M.D. Archer, P680, the primary electron donor of photosystem II, J. Photochem. Photobiol., A 142 (2001) 97–106.
[90] V.I. Prokhorenko, A.R. Holzwarth, Primary processes and structure of the photosystem II reaction center: a photon echo study, J. Phys. Chem., B 104 (2000) 11563–11578.
[91] F. Rappaport, M. Guergova-Kuras, P.J. Nixon, B.A. Diner, J. Lavergne, Kinetics and pathways of charge recombination in photosystem II, Biochemistry 41 (2002) 8518–8527.
[92] C.C. Moser, C.C. Page, P.L. Dutton, Tunneling in PSII, Photochem. Photobiol. Sci. 4 (2005) 933–939.
[93] P. Faller, R.J. Debus, K. Brettel, M. Sugiura, A.W. Rutherford, A. Boussac, Rapid formation of the stable tyrosyl radical in photosystem II, Proc. Natl. Acad. Sci. U. S. A. 98 (2001) 14368–14373.
[94] C. Tommos, G.T. Babcock, Proton and hydrogen currents in photosynthetic water oxidation, Biochim. Biophys. Acta 1458 (2000) 199–219.
[95] J.H. Golbeck, Photosystem I in Cyanobacteria, in: D.A. Bryant (Ed.), Advances in Photosynthesis: The molecular biology of cyanobacteria, Kluwer Academic, Dordrecht, the Netherlands, 1994, pp. 319–360.
[96] M. Guergova-Kuras, B. Boudreaux, A. Joliot, P. Joliot, K. Redding, Evidence for two active branches for electron transfer in photosystem I, Proc. Natl. Acad. Sci. U. S. A. 98 (2001) 4437–4442.
[97] C.C. Moser, P.L. Dutton, Application of Marcus theory to photosystem I electron transfer, in: J.H. Golbeck (Ed.), Photosystem I: the plastocyanin: ferredoxin oxidoreductase in photosynthesis, Kluwer/Springer, New York, in press.
[98] S. Florin, D.M. Tiede, Optical and EPR characterization of reduced bacteriopheophytin redox states in reaction centers of Rps. sphaeroides R-26, in: J. Biggins (Ed.), Prog. Photosynth. Res., vol. 1, Nijhoff, Dorderecht, 1987, pp. 205–208.
[99] C.C. Moser, C.C. Page, P.L. Dutton, Photosynthesis: Bacterial Reaction Center, in: V. Balzani (Ed.), Electron transfer in Chemistry, vol. 3, Wiley-VCH, New York, 2001, pp. 24–38.
[100] W.W. Parson, Z.T. Chu, A. Warshel, Electrostatic control of charge separation in bacterial photosynthesis, Biochim. Biophys. Acta 1017 (1990) 251–272.
[101] J.L. Gao, R.J. Shopes, C.A. Wraight, Charge recombination between the oxidized high-potential C-type cytochromes and Qa- in reaction centers from *Rhodopseudomonas viridis*, Biochim. Biophys. Acta 1015 (1990) 96–108.
[102] L. Krabben, E. Schlodder, R. Jordan, D. Carbonera, G. Giacometti, H.

Lee, A.N. Webber, W. Lubitz, Influence of the axial ligands on the spectral properties of P700 of photosystem I: a study of site-directed mutants, Biochemistry 39 (2000) 13012–13025.
[103] A.W. Rutherford, A. Krieger-Liszkay, Herbicide-induced oxidative stress in photosystem II, Trends Biochem. Sci. 26 (2001) 648–653.
[104] V.A. Shuvalov, The study of the primary photoprocesses in photosystem I of chloroplasts. Recombination luminescence, chlorophyll triplet state and triplet–triplet annihilation, Biochim. Biophys. Acta 430 (1976) 113–121.
[105] N.W.T. Woodbury, W.W. Parson, Nanosecond fluorescence from isolated photosynthetic reaction centers of *Rhodopseudomonas sphaeroides*, Biochim. Biophys. Acta 767 (1984) 345–361.
[106] F.A.M. Kleinherenbrink, G. Hastings, B.P. Wittmershaus, R.E. Blankenship, Delayed fluorescence from Fe–S type photosynthetic reaction centers at low redox potential, Biochemistry 33 (1994) 3096–3105.
[107] R.C. Prince, J.S. Leigh Jr., P.L. Dutton, Thermodynamic properties of the reaction center of *Rhodopseudomonas viridis*. In vivo measurement of the reaction center bacteriochlorophyll-primary acceptor intermediary electron carrier, Biochim. Biophys. Acta 440 (1976) 622–636.
[108] C.A. Wraight, Photochem. Photobiol. 30 (1979) 767–776.
[109] G.N. Johnson, A.W. Rutherford, A. Krieger, A change in the midpoint potential of the quinone Q(a) in photosystem II associated with photoactivation of oxygen evolution, Biochim. Biophys. Acta 1229 (1995) 202–207.
[110] A. Krieger, A.W. Rutherford, G.N. Johnson, On the determination of redox midpoint potential of the primary quinone electron-acceptor, Q(a), in Photosystem II, Biochim. Biophys. Acta 1229 (1995) 193–201.
[111] G. Alegria, P.L. Dutton, Langmuir-blodgett monolayer films of bacterial photosynthetic membranes and isolated reaction centers—Preparation, spectrophotometric and electrochemical characterization 1, Biochim. Biophys. Acta 1057 (1991) 239–257.
[112] K. Brettel, Electron transfer and arrangement of the redox cofactors in photosystem I, Biochim. Biophys. Acta 1318 (1997) 322–373.
[113] H.H. Robinson, A.R. Crofts, Kinetics of the oxidation-reduction reactions of the photosystem II quinone acceptor complex, and the pathway for deactivation, FEBS Lett. 153 (1983) 221–226.
[114] S.K. Chamorovsky, R. Cammack, Direct determination of the midpoint potential of the acceptor-X in chloroplast photosystem—I by electrochemical reduction and electron-spin-resonance spectroscopy, Photobiochem. Photobiophys. 4 (1982) 195–200.
[115] I. Vass, S. Styring, Ph-dependent charge equilibria between tyrosine-D and the S-states in photosystem. 2. Estimation of relative midpoint redox potentials, Biochemistry 30 (1991) 830–839.
[116] R. Edge, E.J. Land, D.J. McGarvey, M. Burke, T.G. Truscott, The reduction potential of the beta-carotene$^{+\cdot}$/beta-carotene couple in an aqueous micro-heterogeneous environment, FEBS Lett. 471 (2000) 125–127.
[117] D.H. Stewart, G.W. Brudvig, Cytochrome b(559) of photosystem II, Biochim. Biophys. Acta 1367 (1998) 63–87.
[118] W.A. Cramer, J. Whitmarsh, Photosynthetic cytochromes, Annu. Rev. Plant Physiol. 28 (1977) 133–172.
[119] H. Ishikita, E.W. Knapp, Redox potentials of chlorophylls and beta-carotene in the antenna complexes of photosystem, J. Am. Chem. Soc. 127 (2005) 1963–1968.
[120] M. Roncel, A. Boussac, J.L. Zurita, H. Bottin, M. Sugiura, D. Kirilovsky, J.M. Ortega, Redox properties of the photosystem II cytochromes b559 and c550 in the cyanobacterium *Thermosynechococcus elongatus*, J. Biol. Inorg. Chem. 8 (2003) 206–216.
[121] R.J. Shopes, L.M.A. Levine, D. Holten, C.A. Wraight, Kinetics of oxidation of the bound cytochromes in reaction centers from *Rhodopseudomonas viridis*, Photosynth. Res. 12 (1987) 165–180.
[122] S. Itoh, M. Iwaki, I. Ikegami, Modification of photosystem I reaction center by the extraction and exchange of chlorophylls and quinones, Biochim. Biophys. Acta 1507 (2001) 115–138.
[123] P. Ball, Natural strategies for the molecular engineer, Nanotechnology 13 (2002) R15–R28.
[124] V. Balzani, A. Credi, M. Venturi, The bottom-up approach to molecular-level devices and machines, Chem. Eur. J. 8 (2002) 5524–5532.
[125] A.K. Chamberlain, S. Faham, S. Yohannan, J.U. Bowie, Construction of helix-bundle membrane proteins, Membr. Proteins 63 (2003) 19–46.
[126] J.U. Bowie, Understanding membrane protein structure by design, Nat. Struct. Biol. 7 (2000) 91–94.
[127] W.F. DeGrado, C.M. Summa, V. Pavone, F. Nastri, A. Lombardi, De novo design and structural characterization of proteins and metalloproteins, Annu. Rev. Biochem. 68 (1999) 779–819.
[128] J.M. Lehn, Toward complex matter: supramolecular chemistry and self-organization, Proc. Natl. Acad. Sci. U. S. A. 99 (2002) 4763–4768.
[129] M.C. Roco, Nanotechnology: convergence with modern biology and medicine, Curr. Opin. Biotechnol. 14 (2003) 337–346.
[130] P.D. Barker, Designing redox metalloproteins from bottom-up and top-down perspectives, Curr. Opin. Struct. Biol. 13 (2003) 490–499.
[131] L. Cristian, V. Nanda, J.D. Lear, W.F. Degrado, Synergistic interactions between aqueous and membrane domains of a designed protein determine its fold and stability, J. Mol. Biol. 348 (2005) 1225–1233.
[132] D. Noy, B.M. Discher, I.V. Rubtsov, R.M. Hochstrasser, P.L. Dutton, Design of amphiphilic protein maquettes: enhancing maquette functionality through binding of extremely hydrophobic cofactors to lipophilic domains, Biochemistry 44 (2005) 12344–12354.
[133] B.M. Discher, R.L. Koder, C.C. Moser, P.L. Dutton, Hydrophillic to amphiphilic design in redox protein maquettes, Curr. Opin. Chem. Biol. 7 (2003) 741–748.
[134] B.M. Discher, D. Noy, J. Strzalka, S. Ye, C.C. Moser, J.D. Lear, J.K. Blasie, P.L. Dutton, Design of amphiphilic protein maquettes: controlling assembly, membrane insertion, and cofactor interactions, Biochemistry 44 (2005) 12329–12343.
[135] S.X. Ye, J. Strzalka, X.X. Chen, C.C. Moser, P.L. Dutton, J.K. Blasie, Assembly of a vectorially oriented four-helix bundle at the air/water interface via directed electrostatic interactions, Langmuir 19 (2003) 1515–1521.
[136] S.X. Ye, J.W. Strzalka, B.M. Discher, D. Noy, S.Y. Zheng, P.L. Dutton, J. K. Blasie, Amphiphilic 4-helix bundles designed for biomolecular materials applications, Langmuir 20 (2004) 5897–5904.